ACS APPLIED MATERIALS & INTERFACES

Research Article

www.acsami.org

Solution-Processed DPP-Based Small Molecule that Gives High Photovoltaic Efficiency with Judicious Device Optimization

Jianhua Huang,[†] Chuanlang Zhan,*[,†] Xin Zhang,[†] Yan Zhao,[§] Zhenhuan Lu,[†] Hui Jia,[†] Bo Jiang,[†] Jian Ye,[†] Shanlin Zhang,[†] Ailing Tang,[†] Yunqi Liu,[§] Qibing Pei,[‡] and Jiannian Yao*[,†]

[†]Beijing National Laboratory for Molecular Sciences, CAS Key Laboratory of Photochemistry, Institute of Chemistry, and [§]CAS Key Laboratory of Organic Solids, Institute of Chemistry, Chinese Academy of Sciences, Beijing 100190, P.R. China

[‡]Department of Materials Science and Engineering, University of California at Los Angeles, Los Angeles, California 90095, United States

Chinese Academy of Sciences, Beijing, 100190, P.R. China

Supporting Information

ABSTRACT: A solution-processed diketopyrrolopyrrole (DPP)-based small molecule, namely BDT-DPP, with broad absorption and suitable energy levels has been synthesized. The widely used solvents of chloroform (CF) and *o*-dichlorobenzene (*o*-DCB) were used as the spin-coating solvent, respectively, and 1,8-diiodooctane (DIO) was used as additive to fabricate efficient photovoltaic devices with BDT-DPP as the donor material and PC71BM as the acceptor material. Devices fabricated from CF exhibit poor fill factor (FF) of 43%, low short-circuit current density (J_{sc}) of 6.86 mA/cm^2, and moderate power conversion efficiency (PCE) of 2.4%, due to rapid evaporation of CF, leading to poor morphology of the active layer. When 0.3% DIO was added, the FF and J_{sc} were improved to 60% and 8.49 mA/cm^2, respectively, because of the better film morphology. Active layer spin-coated from the high-boiling-point solvent of *o*-DCB shows better phase separation than that from CF, because of the slow drying nature of *o*-DCB, offering sufficient time for the self-organization of active-layer. Finally, using *o*-DCB as the parent solvent and 0.7% DIO as the cosolvent, we obtained optimized devices with continuous interpenetrating network films, affording a J_{sc} of 11.86 mA/cm^2, an open-circuit voltage (V_{oc}) of 0.72 V, an FF of 62%, and a PCE of 5.29%. This PCE is, to the best of our knowledge, the highest efficiency reported to date for devices prepared from the solution-processed DPP-based small molecules.

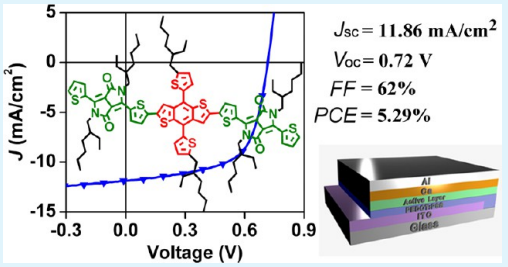

KEYWORDS: *solution-processed small molecules, diketopyrrolopyrrole, organic solar cells, device optimization*

1. INTRODUCTION

Solution-processed organic solar cells (OSCs), which involve bulk heterojunction of an organic donor material and a fullerene derivative, have been intensively researched recently because of their potential to afford green energy.[1] Along with great efforts on molecular design, device optimization, and device structure innovation, a large amount of polymer materials with high power conversion efficiency (PCE) of 6–8% have been developed.[2−6] Compared to the well-developed polymer materials, small molecules have been less investigated and the efficiency is commonly inferior to that of polymer solar cells.[7] Although a high efficiency of ∼7% has been reported recently from several molecules,[8−10] building the molecular tool-box for highly efficient small molecules remains urgent. Currently, the sorts of solution-processed small molecules with high efficiency, typically, > 4% are still countable, for example: (I) bow-shaped molecules based on silole and pyridyl[2,1,3]-thiadiazole;[8,9] (II) star molecules based on triphenylamine;[11] (III) oligomeric thiophene or its derivatives end-capped with electron-deficient units;[10,12,13] (IV) dye molecules based on diketopyrrolopyrrole (DPP).[14−17] Among those outstanding materials, DPP-based molecules are promising candidates due to the favorable properties of the DPP unit, e.g., strong light absorption, photochemical stability, excellent charge carrier mobility, and easy synthesis.[14,18−24] However, photovoltaic performances of the DPP-based molecules reported to date were not satisfying. High-efficiency solar cells made from DPP-based molecules were really rare and the highest PCE reported to date was still below 5%.[15,17] Can the high efficiency be achieved from DPP-based molecules and how can it be achieved?

Despite that the novel molecular structures with excellent optoelectronic properties are important for high efficient solar cells, conditions for device optimization is also a key factor determining the efficiency. Currently, basic device optimization strategies include the thermal annealing,[25,26] solvent annealing,[27,28] high-boiling-point solvent additives,[29,30] and altering the spin-coating solvent,[31] all of which are for the purpose of

Received: November 29, 2012
Accepted: February 21, 2013
Published: February 21, 2013

improving the donor/acceptor phase separation and creating effective pathways for the charge carrier transport. For the solution-processed small molecules, the spin-coating solvent, including the parent solvent and the small amount additives, is of vital importance to obtain a well-coated active layer. At present, the widely used solvents for spin-coating are chloroform (CF) and *o*-dichlorobenzene (*o*-DCB) because of their good solubility to most of the organic molecules. High efficient devices fabricated from both of the two solvents have been reported. For example, a DPP-based small molecule end-capped with benzofuran exhibited an efficiency of 4.8% with CF as the spin-coating solvent.[17] Equally, bow-shape molecule based on silole and pyridyl[2,1,3]thiadiazole gave a PCE of 6.7%, spin-coated with *o*-DCB.[8] Although both of the solvents possess advantages to prepare solar cells for different devices, why and how the device performances differ from each other so much is not well addressed.

In this paper, we selected the two-dimensional conjugate unit of benzodithiophene (BDT) as the donor unit, while two DPP units as the acceptor units, both covalently attached onto the ends of BDT. Six 2-ethylhexyl (EH) groups were attached to the backbone to ensure the solubility, and finally forming BDT-DPP, an A-D-A type DPP-based small molecule, as shown in Scheme 1. On the basis of this molecule, photovoltaic devices

Scheme 1. Molecular Structure of BDT-DPP

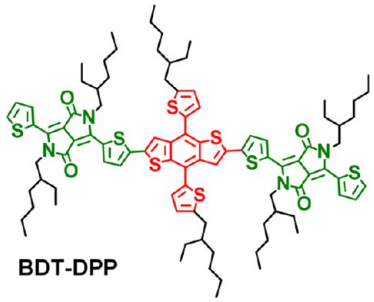

were fabricated with CF and *o*-DCB, respectively, as the parent solvent, and the commonly used high-boiling additive 1,8-diiodooctane (DIO) as the cosolvent. The results indicated that the devices prepared from the low-boiling CF exhibit a low fill factor (FF) and poor short-circuit current density (J_{sc}), due to the rapid evaporation, leading to poor morphology of the active layer. When 0.3% DIO was added, the FF and J_{sc} were both improved because of the better film morphology. Compared to CF, active layer spin-coated from the high boiling-point *o*-DCB afforded better FF and J_{sc}. Furthermore, when 0.7% DIO was added to the *o*-DCB solution, the PCE of the device further enhanced. Finally, after various optimizations, a PCE of 5.29%, with a J_{sc} of 11.86 mA/cm^2, an open-circuit voltage (V_{oc}) of 0.72 V, and an FF of 62% was obtained. This PCE is, to the best of our knowledge, the highest efficiency reported to date for devices prepared from the solution-processed DPP-based small molecules.

2. RESULTS AND DISCUSSION

2.1. Synthesis. BDT-DPP was synthesized according to Scheme 2. The starting material 2,6-bis(trimethyltin)-4,8-bis(octyloxyl)benzo[1,2-b;4,5-b′]dithiophene (**1**) was purchased from Solarmer and 3-(5-bromothiophen-2-yl)-2,5-bis-(2-ethylhexyl)-6-(thiophen-2-yl)pyrrolo[3,4-c] pyrrole-1,4-(2H,5H)-dione (**2**) was synthesized according to the literature

Scheme 2. Synthetic Route to BDT-DPP[a]

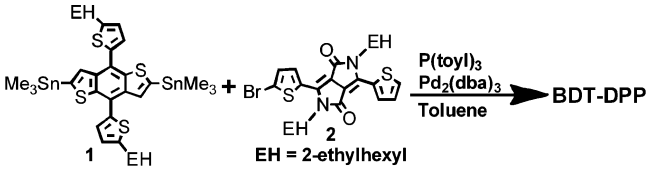

[a]Conditions: $P(toyl)_3$, $Pd_2(dba)_3$, toluene, reflux under 120 °C, overnight.

method.[16] Stilling coupling reaction between **1** and **2** produced BDT-DPP with a yield of 82%. The final product was fully characterized with ^{1}H NMR, ^{13}C NMR, TOF-MS, and elemental analysis. BDT-DPP exhibits good solubility (>15 mg/mL) in CF and *o*-DCB. The decomposed temperature at 5% weight loss for BDT-DPP is 409 °C, as shown in Figure S1 in the Supporting Information, which is thermal stable enough for device fabrication. Differential scanning calorimetry (DSC) was tested to study the thermal transitions of BDT-DPP. As shown in Figure S2 in the Supporting Information, melting temperature of BDT-DPP was observed to be 287 °C. Two exothermic peaks at 270 and 262 °C were observed, which may be attributed to the monotropic liquid crystalline behavior.[32]

2.2. Optoelectronic Properties. Figure 1a shows absorption spectra of pure BDT-DPP in CF and in film. The

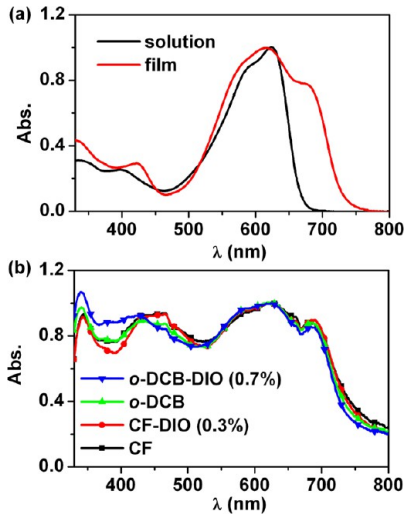

Figure 1. (a) UV−vis absorption spectrum of BDT-DPP in CF and film, and (b) the blended film absorption of BDT-DPP/PC71BM (1:1, weight ratio), prepared using different solvents.

solution absorption maximum (λ^a_{max}) locates at 624 nm with a full width at half-maximum (fwhm) of 104 nm. The film absorption is broadened with a larger fwhm of 167 nm and the λ^a_{max} is slightly blue-shifted to 617 nm with a shoulder emerging at a much red-shifting wavelength of 676 nm, indicating strong molecule stacking in the solid state. The optical bandgap (E_g^{opt}) calculated from the film absorption edge is 1.64 eV (1240/755). Figure 1b shows the absorption of BDT-DPP/PC71BM blended films mixed in a 1:1 weight ratio and spin-coated with CF, CF-DIO, *o*-DCB, *o*-DCB-DIO as the solvent, respectively, which will implement in the device preparations. The blended film exhibits a full coverage from 330 to 800 nm, indicating the high light-harvesting ability of the active layer. Compared to the absorption of pure BDT-DPP, the absorption band from 330 to

450 mainly results from the PC71BM.[17] The relative absorbance strength from 330 to 450 is increased under the following sequence: CF < CF-DIO, *o*-DCB < *o*-DCB-DIO. That result can be ascribed to the strong interaction between PC71BM and DIO,[29] which makes the PC71BM domain more ordered.

Figure 2a shows the cyclic voltammograms (CV) of BDT-DPP film with Ag/AgCl as a reference electrode. The highest

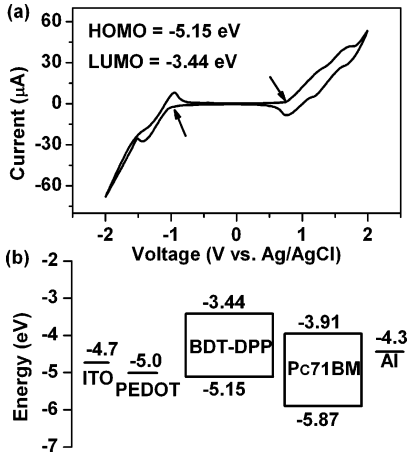

Figure 2. (a) Cyclic voltammograms of BDT-DPP in $CHCl_3$/0.1 M Bu_4NBF_6 at 100 mV/s and (b) energy levels of different components in a photovoltaic device.

occupied molecular orbital (HOMO) and the lowest unoccupied molecular orbital (LUMO) are estimated from the empirical equation of $E_{HOMO/LUMO} = -(E_{onset\ (ox/red)} + 4.4)$ eV[33,34] to be −5.15 and −3.44 eV, respectively. That energy levels match well with the acceptor material of PC71BM,[35,36] as shown in Figure 2b. The electrochemical bandgap is 1.71 eV, which is consistent with the optical bandgap.

2.3. Photovoltaic Performances. To evaluate the photovoltaic performances of BDT-DPP, we fabricated OSCs using BDT-DPP as the donor material and PC71BM as the acceptor material with the traditional architecture of ITO/PEDOT:PSS/BDT-DPP:PC71BM/Ca/Al. CF and *o*-DCB were used as the spin-coating solvent, respectively. A small amount of DIO was used as additive to improve the phase separation. The device results are summarized in Table 1. The best efficiency was given and the average efficiency from 5 devices was also given. First, CF was used to spin-cast the active layer with various donor/acceptor ratios. When the D/A ratio increased form 1:1 to 2:1, 3:1, and 4:1, the J_{sc} and FF values decreased apparently. When the D/A ratio descended from 1:1 to 1:2, 1:3, and 1:4, the FF retained and J_{sc} declined slightly. The best device was obtained when the D/A ratio was 1:1, affording a J_{sc} of 6.86 mA/cm^2, a V_{oc} of 0.84 V, an FF of 43%, and an average PCE of 2.43%. We have to note that most of high efficient small molecules exhibit best device results when the D/A ratios were higher than 1:1.[8,10,12,13] However, in our system, the D/A ratio increasing may produce thicker active layer and hinder the charge transport to electrodes,[37] leading to poor *FF* and J_{sc}. The D/A ratio decreasing may weaken the light absorption, giving rise to declined J_{sc}. The high V_{oc}, which was stable as the D/A ratio altered, is related to the deep HOMO (−5.15 eV) of BDT-DPP. On the basis of the D/A ratio of 1:1 with CF as parent solvent, different amounts of DIO were added to improve the phase separation. Incorporating 0.3% DIO into the active

Table 1. Photovoltaic Performances Based on BDT-DPP/PC71BM

	DIO%	D/A ratio	Jsc (mA/cm^2)	V_{oc} (V)	FF	*PCE* (avg %)
CF		80:20	1.56	0.86	0.21	0.29(0.25)
		70:30	3.29	0.83	0.27	0.74(0.70)
		60:40	4.20	0.87	0.30	1.10(1.05)
		50:50	6.86	0.84	0.43	2.47(2.43)
		40:60	6.23	0.80	0.41	2.07(2.02)
		30:70	6.11	0.81	0.45	2.24(2.20)
		20:80	5.70	0.77	0.31	1.37(1.32)
	0.1	50:50	7.66	0.75	0.55	3.17(3.12)
	0.3	50:50	8.49	0.76	0.60	3.88(3.82)
	0.5	50:50	7.62	0.74	0.56	3.18(3.12)
o-DCB		40:60	8.05	0.72	0.50	2.89(2.80)
		50:50	8.63	0.73	0.56	3.53(2.48)
		60:40	6.92	0.72	0.39	1.95(1.88)
		70:30	5.53	0.74	0.42	1.73(1.69)
		80:20	4.53	0.75	0.37	1.27(1.23)
	0.1	50:50	9.20	0.73	0.62	4.15(4.07)
	0.3	50:50	9.79	0.72	0.61	4.30(4.23)
	0.5	50:50	9.80	0.72	0.61	4.30(4.21)
	0.7	50:50	11.86	0.72	0.62	5.29(5.15)
	0.9	50:50	10.85	0.73	0.62	4.92(4.86)

solution gave best device results, with a J_{sc} of 8.49 mA/cm^2, a V_{oc} of 0.76 V, an *FF* of 60%, and a PCE of 3.88%. Typically, the concentrations of high boiling-point solvent in polymer solutions range between 1% and 5% (v/v).[38] However, in our system, when the DIO concentration increased to 1%, the devices were totally deteriorated, giving typical diodelike curves.

Subsequently, *o*-DCB was used as the spin-coating solvent. The trend of the device results depending on the D/A ratios was similar to that of the devices made from CF. After various D/A ratio optimizations, the best PCE occurred when the D/A ratio was 1:1, giving a J_{sc} of 8.63 mA/cm^2, a V_{oc} of 0.73 V, an FF of 56%, and a *PCE* of 3.53%. On the basis of the D/A ratio of 1:1, various amounts of DIO were incorporated in the active solution, as shown in Table 1. When the DIO content was 0.7%, the device gave the highest PCE of 5.29%, with a J_{sc} of 11.86 mA/cm^2, a V_{oc} of 0.72 V, and an FF of 62%, which is the highest efficiency reported to date for devices prepared from the solution-processed DPP-based small molecules. It is also worth noting that the increased *FF* of 62%, which results from the favorable phase separation and the high hole mobility, as discussed in the following contents, is among the highest rank for solution-processed small molecules.[8,10] We also have to note that any annealing procedures (e.g., solvent annealing, thermal annealing) totally deteriorate the devices, affording diodelike curves, which probably result from the over-aggregation of D/A domains.

Through various device optimizations, we obtained four champion devices fabricated from CF, CF-DIO (0.3%), *o*-DCB, and *o*-DCB-DIO (0.7%) with *PCE*s of 2.47, 3.88, 3.53, and 5.29%, respectively, as shown in Figure 3. To get insights into the origins that cause the differences of device efficiency, we carried out various characterizations on the active-layers that prepared under the four spin-coating conditions, as displayed in the following discussions.

The external quantum efficiency (EQE) of the optimized devices prepared from CF, CF-DIO (0.3%), *o*-DCB, and *o*-DCB-DIO (0.7%) were tested, as shown in Figure 4. All the

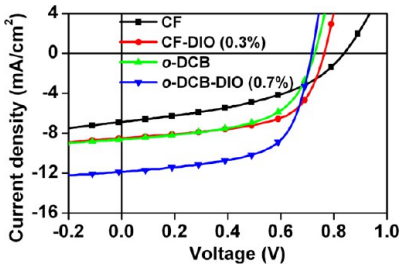

Figure 3. $J-V$ curves of the champion devices prepared from CF, CF-DIO (0.3%), *o*-DCB, and *o*-DCB-DIO (0.7%), respectively.

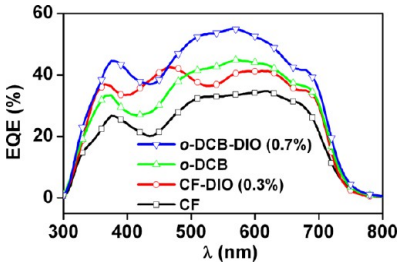

Figure 4. External quantum efficiency (EQE) curves of the champion devices fabricated from CF, CF-DIO (0.3%), *o*-DCB, and *o*-DCB-DIO (0.7%), respectively.

four curves exhibit a broad response from 300 to 800 nm and are consistent with their respective UV−vis absorption profile (Figure 1b), indicating the absorbed photons contribute to the photovoltaic conversion. The maximum monochromatic EQE are 35, 43, 45, and 55% for the devices prepared from CF, CF-DIO (0.3%), *o*-DCB, and *o*-DCB-DIO (0.7%), respectively. The J_{sc} calculated from the integral of EQE curves are consistent with the J_{sc} value obtained from the $J-V$ curves.

2.4. Molecule Stacking. To investigate the molecule stacking in the solid state, XRD of the pristine BDT-DPP and BDT-DPP/PC71BM blended film was tested on silica and ITO/PEDOT: PSS substrate, respectively. Figure 5a shows the XRD patterns of pristine BDT-DPP, PC71BM, and BDT-DPP/PC71BM blends on silica by drop-casting. Pristine BDT-DPP film displays high crystallinity with ordered three-dimensional stacking. The diffraction degree (2θ) of the *a*, *b*, and *c* directions were located at 4.54, 6.10, and 23.02°, representing the stacking distances of 19.5, 15.5, and 3.9 Å, respectively. According to the theoretical calculations, *a*, *b*, and *c* stacking directions correspond to the orientations along the directions of the backbone, alkyl chain, and $\pi-\pi$ stacking, respectively, as schematically shown in Figure 5b. It is worth noting that along the alkyl chain direction (*b* direction), there are obvious second-order diffraction (**2b**) and three-order diffraction (**3b**), indicating highly ordered organization of pure BDT-DPP in the solid state. The ordered three-dimensional stacking of BDT-DPP in film primarily results from the regular appending of alkyl chains and the strong intermolecular interactions between the DPP and BDT units.

After blending with PC71BM, ordered stacking in the *a* direction is retained (Figure 5a, red line). However, the loss of the higher ordered diffractions along the *b* direction suggests that the BDT-DPP network is interrupted by PC71BM. Similarly, the diffraction pattern of PC71BM is also obvious less featured after blending with BDT-DPP, indicating good miscibility of BDT-DPP and PC71BM. Both the variations of the BDT-DPP and PC71BM diffraction patterns imply the

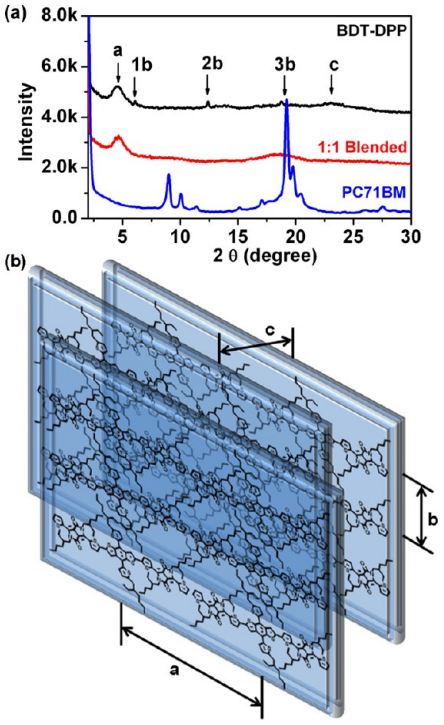

Figure 5. (a) XRD patterns of the pristine BDT-DPP (black), PC71BM (blue), and BDT-DPP/PC71BM (red) films and (b) schematic model of the pristine BDT-DPP in the solid state.

formation of the donor and acceptor domains, which are essential for the hole and electron transport.

We also prepare the XRD samples with the same conditions as the device fabrication on ITO/PEDOT: PSS substrate, with CF, CF-DIO (0.3%), *o*-DCB, and *o*-DCB-DIO (0.7%) as spin-coating solvent, respectively. As shown in Figure S2 in the Supporting Information, only when *o*-DCB-DIO (0.7%) was utilized to spin-coat the active layer, the XRD pattern show obvious diffraction along the *a* direction, implying a more ordered stacking of BDT-DPP and effective hole transport path, which is consistent with the high efficiency and anticipates high hole mobility (vide post).

2.5. Hole Mobility. Hole mobilities of BDT-DPP/PC71BM films, which prepared from CF, CF-DIO (0.3%), *o*-DCB, and *o*-DCB-DIO (0.7%) were evaluated using the space-charge limited current (SCLC) model.[18,39−42] The experimental details are described in the Experimental Section. As shown in Figure 6, the average hole mobilities for films casting from CF, CF-DIO (0.3%), *o*-DCB, and *o*-DCB (0.7% DIO) were

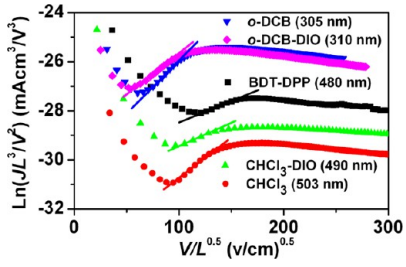

Figure 6. Plots of $\ln(JL^3/V^2)$ vs $(V/L)^{0.5}$ of the pristine BDT-DPP film and BDT-DPP/PC71BM prepared from CF, CF-DIO (0.3%), *o*-DCB, and *o*-DCB-DIO (0.7%), respectively. The film thickness is shown in brackets.

found to be 7.76×10^{-4} $cm^2/(V\ s)$, 3.47×10^{-2} $cm^2/(V\ s)$, 1.41×10^{-1} $cm^2/(V\ s)$, and 4.67×10^{-1} $cm^2/(V\ s)$, respectively. Compared to the CF spin-coated device, the hole mobility of CF-DIO (0.3%) spin-coated device improved by two magnitude, which is consistent with the favorable phase separation by using CF-DIO (0.3%), as discussed in the following AFM and TEM data. Devices prepared from *o*-DCB and *o*-DCB -DIO (0.7%) exhibit a further higher hole mobility of 1.41×10^{-1} $cm^2/(V\ s)$, and 4.67×10^{-1} $cm^2/(V\ s)$, which is among the highest rank in small molecule donors. In order to demonstrate the reliability of those values, we also test the hole mobility of the pristine BDT-DPP film with the SCLC model. As shown in Figure 6 (black plots), the pristine BDT-DPP film exhibited a hole mobility of 1.75×10^{-1} $cm^2/(V\ s)$. Furthermore, organic thin-film transistors (OTFTs) were also fabricated with bottom contact configurations to evaluate the hole mobility of the pristine BDT-DPP film. Output and transfer curves are shown in Figure S4 in the Supporting Information, and the hole mobility of BDT-DPP were estimated to be 4.0×10^{-2} $cm^2/V{\cdot}s$. We have to point out that the hole mobilities of the pristine BDT-DPP films derived from the SCLC model and OTFT method were slightly different, which were probably originated from the different molecular orientation of BDT-DPP in OTFTs and photovoltaic devices.[43−45] We attribute the higher hole mobility of devices prepared with *o*-DCB than that of CF to the higher boiling-point of *o*-DCB, offering more time for BDT-DPP to self-organization within the active layer and then form more ordered packing, as revealed from the XRD patterns (see Figure S3 in the Supporting Information), which will be demonstrated in the AFM and TEM data.

2.6. Film Morphology. The surface morphology of the BDT-DPP/PC71BM blended films, respectively, spin-coated from CF, CF-DIO (0.3%), *o*-DCB, and *o*-DCB-DIO (0.7%) were studied by tapping-mode atomic force microscopy (AFM). Figure S5 in the Supporting Information shows the height images collected from the device films prepared with the four solvents. The root-mean-square (rms) roughness of the four blend films were 0.50, 0.89, 0.75, and 2.65 nm, respectively. Phase images of the four films show different features, as shown in Figure 7. The CF spin-coated film shows isolated spherical domains with sizes of 30−50 nm (Figure 7a). When 0.3% DIO was used as the cosolvent, the spherical morphologies are retained well with a bit reduction in size. Most important is the occurrence of the continuous amorphous phase, which interpenetrate in between the spherical domains, indicating efficient nanoscale phase separation formed (Figure 7b), which is favorable for the charge transportation, offering improved PCE. Blend films spin-coated from *o*-DCB also showed a continuous amorphous phase, surrounding around the spherical domains (Figure 7c), probably due to the slower drying nature of *o*-DCB, offering more time for the molecular stacking. Finally, for the *o*-DCB-DIO (0.7%) spin-coated film, the spherical domains were connected by the continuous but much smaller amorphous phase, forming interpenetrating network, without changing the scale of the basic spherical domains with the sizes ranging from 30 to 50 nm (Figure 7d), indicating the formation of efficient percolation of channels for charge transport, consistent with its highest efficiency and hole mobility.

Transmission electron microscopy (TEM) was used to study the bulk phase separation of the blend films. As shown in Figure 8, the bright regions can be attributed to the BDT-DPP domains, whereas the dark regions can be attributed to the PC71BM domains due to its high electron scattering density.[46] Phase separation in the bulk of the CF spin-coated film was ambiguous (Figure 8a), whereas the CF-DIO (0.3%) spin-coated film exhibited two distinct feature types (Figure 8b). Similarly, phase separation in *o*-DCB-DIO (0.7%) spin-coated film was more significant than the *o*-DCB spin-coated film (Figure 8c and 8d). This trend indicated that the addition of DIO as cosolvent helps the self-organization of the active layer and produces continuous interpenetrating network films, which is essential for the exciton separation and charge transport. It is worthy noting that the *o*-DCB-DIO (0.7%) spin-coated film exhibit continuous nanoscale phase separation about 30−50 nm, which is approaching to the optimum exciton diffusion length,[47] consistent with its enhanced PCE.

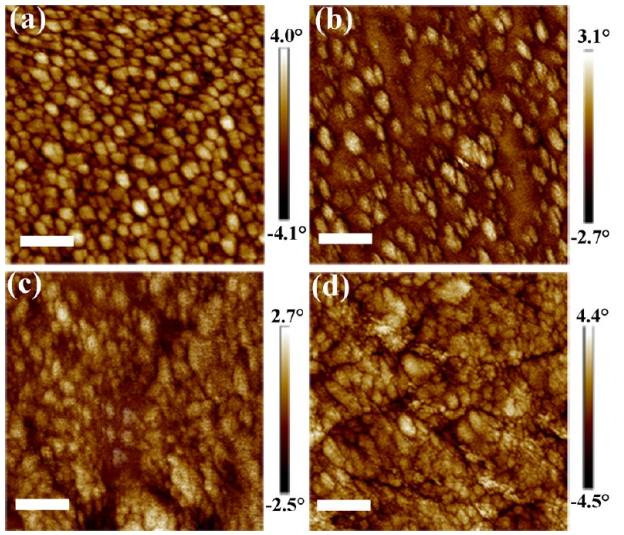

Figure 7. AFM phase images of the BDT-DPP/PC71BM blended films prepared from (a) CF, (b) CF-DIO (0.3%), (c) *o*-DCB, and (d) *o*-DCB-DIO (0.7%), respectively. The scar bars represent 200 nm.

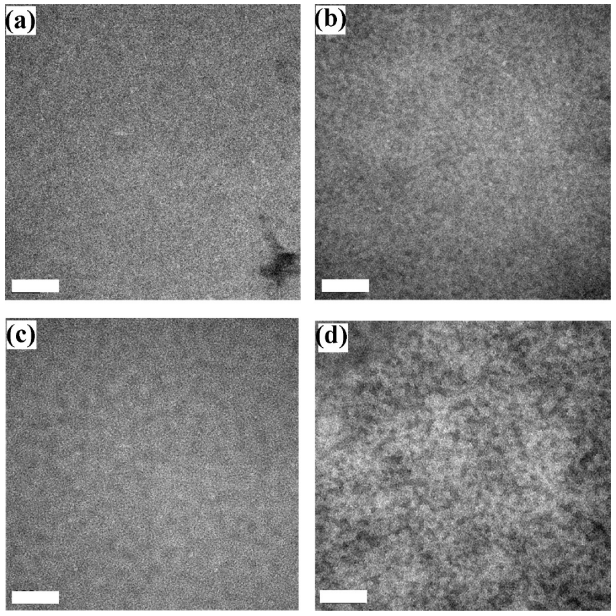

Figure 8. TEM images of the BDT-DPP/PC71BM blended films prepared from (a) CF, (b) CF-DIO (0.3%), (c) *o*-DCB, and (d) *o*-DCB-DIO (0.7%), respectively. The scale bars represent 200 nm.

3. CONCLUSIONS

A solution-processed small molecule based on two-dimensional benzodithiophene (BDT) and DPP, namely, BDT-DPP was synthesized. The A-D-A type molecule has broad absorption and exhibits the HOMO level of −5.15 eV and the LUMO level of −3.44 eV, which both match well with that of PC71BM. Chloroform (CF) and *o*-dichlorobenzene (*o*-DCB) were used as the spin-coating solvent, respectively and 1,8-diiodooctane (DIO) was used as additive to fabricate photovoltaic devices with BDT-DPP as the donor material and PC71BM as the acceptor material. Low boiling-point CF fabricated devices with poor fill factor (FF) of 43%, low short-circuit current density (J_{sc}) of 6.86 mA/cm^2, and medium power conversion efficiency (PCE) of 2.4%, due to rapid drying nature of CF, leading to poor morphology of the active layer. Incorporating 0.3% DIO as cosolvent improved the devices performances due to improvement of film morphology. Devices prepared from *o*-DCB shows better phase separation than that of CF, owing to the slow drying of solvent, offering sufficient time for the self-organization of active-layer. Finally, using *o*-DCB as the parent solvent, 0.7% DIO as the cosolvent, optimized devices with continuous interpenetrating network films were obtained, affording a J_{sc} of 11.86 mA/cm^2, an open-circuit voltage (V_{oc}) of 0.72 V, an FF of 62%, and a PCE of 5.29%. This PCE is the highest efficiency reported to date from the solution-processed DPP-based small molecules. Accordingly, our results reveal that suitable molecular design, for example, incorporation of the 2D conjugated donor unit in between two DPP moieties, and careful optimizations of the film morphologies by changing the spin-coating solvents with different boiling-points and accompanying with the utilizations of high boiling-point cosolvent will be one way toward high efficient DPP-based small molecules.

4. EXPERIMENTAL SECTION

4.1. Measurements and Characterizations. The ^{1}H NMR and ^{13}C NMR spectra were measured on a Bruker AVANCE 400 MHz spectrometer using tetramethylsilane (TMS; δ 0 ppm) as an internal standard. Mass spectra (MALDI-TOF-MS) were determined on a Bruker BIFLEX III mass spectrometer. Elemental analysis was performed on a flash EA1112 analyzer. Thermogravimetric analysis (TGA) was performed on a Perkin-Elmer TGA-7 at a heating rate of 10 °C/min under nitrogen flow. Differential scanning calorimetry (DSC) were tested on a Diamond DSC 822e with a heating rate of 10 °C/min. UV−vis absorption was recorded on a Hitachi U-3010 spectrometer. The electrochemical measurements were carried out in a deoxygenated solution of tetra-n-butylammonium hexafluorophosphate (0.1 M) in $CHCl_3$ with a computer-controlled Zennium electrochemical workstation. A glassy carbon electrode, a Pt wire, and an Ag/AgCl electrode were used as the working, counter, and reference electrodes, respectively. AFM images were obtained from the photovoltaic device samples using a Nanoscope V AFM (Digital Instruments) in tapping mode. TEM tests were performed on a JEM-2011F operated at 200 kV. The TEM specimens were prepared by transferring the spin-coated films to the 200 mesh copper grids. The XRD pattern was recorded by a Rigaku D/max−2500 diffractometer operated at 40 kV voltage and a 200 mA current with Cu Kα radiation.

4.2. Fabrications and Characterizations of Organic Solar Cells. The organic solar cells (OSCs) devices were fabricated with the traditional configurations of ITO/PEDOT: PSS/Polymer/PCBM/Ca/Al. The indium tin oxide (ITO) glass was precleaned, respectively, with deionized water, acetone and isopropanol and treated in a Novascan PSD-ultraviolet-ozone chamber for 30 min. A thin layer (ca. 30 nm) of poly(3,4-ethylene-dioxythiophene):poly(styrenesulfonate) (PEDOT:PSS, Baytron P VP AI 4083, Germany) was spin-coated onto the ITO glass with spin-coating speed of 2000 rpm and baked at 150 °C for 10 min. A solution of BDT-DPP/PC71BM with CF, CF-DIO, *o*-DCB, and *o*-DCB-DIO as solvent, respectively, was subsequently spin-coated on the surface of the PEDOT: PSS layer to form a photosensitive layer. Then, the Ca/Al cathode was deposited on the photoactive layer by vacuum evaporation (ca. 20/80 nm). The thickness of active layers are in the range of 100−120 nm with CF as spin-coating solvent and 160−180 nm with *o*-DCB as spin-coating solvent. The effective area of one cell is 6 mm^2. The current−voltage (I−V) measurement of the devices was conducted on a computer-controlled Keithley 2400 Source Measure Unit. A xenon lamp with AM1.5 filter was used as the white light source, and the optical power at the sample was 100 mW/cm^2. EQE measurements were carried out on an oriel IQE 200 (Newport).

4.3. Tests of the Hole Mobilities of BDT-DPP/PC71BM. The devices were fabricated with configuration of ITO/PEDOT: PSS/BDT-DPP: $PC_{71}BM$/Au. The Au layer was deposited under a low speed (1 Å/10 s) to avoid the penetration of Au atoms into the active layer. The active layers were spin-coated with CF, CF-DIO (0.3%), *o*-DCB, *o*-DCB-DIO (0.7%), respectively. The following equation was applied to estimate the hole mobilities:[39,41] $\ln(JL^3V^2) = 0.89(1/E_0)^{0.5}(V/L)^{0.5} + \ln(9\varepsilon\varepsilon_0\mu_0/8)$, where ε is the dielectric constant of the polymer, ε_0 the permittivity of the vacuum, μ_0 the zero-field mobility, E_0 the characteristic field, J the current density, L the thickness of the films, and $V = V_{appl} - V_{bi}$; V_{appl} is the applied potential, and V_{bi} the built-in potential which results from the difference in the work function of the anode and the cathode (in this device structure, V_{bi} = 0.2 V). The hole mobility of the blending films were deduced from the intercept value $\ln(9\varepsilon\varepsilon_0\mu_0/8)$. Herein, ε is 3 and ε_0 is 8.85419 × 10^{-12} C V^{-1} m^{-1}.

4.4. Materials. All of the starting materials and solvents were purchased from Sigma Aldrich or Alfa Aesar and were used without further purification, unless otherwise stated. Tetrahydrofuran (THF) and toluene were distilled from sodium benzophenone ketyl under nitrogen before use. The starting material 2,6-bis(trimethyltin)-4,8-bis(octyloxyl)benzo[1,2-b;4,5-b′]dithiophene (**1**) was purchased from Solarmer and 3-(5-bromothiophen-2-yl)-2,5-bis(2-ethylhexyl)-6-(thiophen-2-yl)pyrrolo[3,4-c] pyrrole-1,4(2H,5H)-dione (**2**) was synthesized according to the literature method.[16]

4.5. Synthesis and Characterizations of BDT-DPP. Starting materials **1**, **2**, and tri(o-tolyl)phosphine were dissolved in dry toluene and degassed with N_2 for 10 min. Then, tris(dibenzylideneacetone)-dipalladium was added. The mixture was stirred at 120 °C overnight under the N_2 atmosphere. After being cooled to room temperature, toluene was then evaporated using a rotary evaporator. The residue was purified by column chromatography on silica gel (petrol ether/dichloromethane = 1:1) to give BDT-DPP black solid in a yield of 82%. ^{1}HNMR (400 MHz, $CDCl_3$): 9.20 (quartet, 4H, J_1 = 4, J_2 = 3.2), 7.80 (d, 2H, J = 7.2), 7.62 (d, 2H, J = 5.2), 7.42 (d, 2H, J = 4), 7.35 (d, 2H, J = 3.2), 7.28 (s, 2H), 6.96 (d, 2H, J = 3.6), 4.04 (t, 8H, J_1 = 6.4, J_2 = 6), 2.91 (d, 4H, J = 6.8), 1.87 (t, 4H, J_1 = 6.4, J_2 = 6.8), 1.74 (t, 2H, J_1 = 5.6, J_2 = 4.8), 1.24−1.49 (m, 48H), 0.85−0.98 (m, 36H). ^{13}C NMR (100 MHz, $CDCl_3$): 161.79, 161.68, 146.58, 142.48, 140.23, 139.64, 139.38, 137.67, 137.10, 136.82, 136.50, 135.54, 130.66, 129.99, 129.47, 128.60, 128.23, 126.36, 125.79, 124.03, 120.88, 108.58, 108.32, 46.10, 46.01, 41.61, 39.47, 39.27, 34.54, 32.73, 30.54, 30.38, 29.11, 28.70, 28.50, 25.93, 23.86, 23.71, 23.24, 23.22, 19.01, 14.36, 14.24, 14.19, 11.09, 10.76, 10.66, 10.47. MS (MALDI-TOF): calculated for $C_{94}H_{118}N_4O_4S_8$, 1622.69; found m/z 1623.60 (M+H$^+$). Anal. Calcd for $C_{94}H_{118}N_4O_4S_8$ (%): C, 69.50; H, 7.32; N, 3.45. Found (%): C, 69.53; H, 7.30; N, 3.47.

■ ASSOCIATED CONTENT

Ⓢ Supporting Information

^{1}HNMR spectra, ^{13}CNMR spectra, TGA curves, DSC curves, XRD, AFM height images, OTFT output, and transfer curves. This material is available free of charge via the Internet at http://pubs.acs.org.

AUTHOR INFORMATION

Corresponding Author

*E-mail: clzhan@iccas.ac.cn (C.Z.); jnyao@iccas.ac.cn (J.Y.).

Author Contributions

The manuscript was written through contributions of all authors. All authors have given approval to the final version of the manuscript.

Notes

The authors declare no competing financial interest.

ACKNOWLEDGMENTS

This work was financially supported by NSFC (Nos. 20973182 and 91227112), the Chinese Academy of Sciences, Project 973 (2011CB808400).

REFERENCES

(1) Thompson, B. C.; Frechet, J. M. *Angew. Chem., Int. Ed.* **2008**, *47*, 58.
(2) Chen, H. Y.; Hou, J. H.; Zhang, S. Q.; Liang, Y. Y.; Yang, G. W.; Yang, Y.; Yu, L. P.; Wu, Y.; Li, G. *Nat. Photon.* **2009**, *3*, 649.
(3) Dou, L. T.; You, J. B.; Yang, J.; Chen, C. C.; He, Y. J.; Murase, S.; Moriarty, T.; Emery, K.; Li, G.; Yang, Y. *Nat. Photon.* **2012**, *6*, 180.
(4) He, Z.; Zhong, C.; Huang, X.; Wong, W. Y.; Wu, H.; Chen, L.; Su, S.; Cao, Y. *Adv. Mater.* **2011**, *23*, 4636.
(5) Huo, L.; Hou, J.; Zhang, S.; Chen, H. Y.; Yang, Y. *Angew. Chem., Int. Ed.* **2010**, *49*, 1500.
(6) Liang, Y.; Xu, Z.; Xia, J.; Tsai, S. T.; Wu, Y.; Li, G.; Ray, C.; Yu, L. *Adv. Mater.* **2010**, *22*, E135.
(7) Walker, B.; Kim, C.; Nguyen, T.-Q. *Chem. Mater.* **2011**, *23*, 470.
(8) Sun, Y. M.; Welch, G. C.; Leong, W. L.; Takacs, C. J.; Bazan, G. C.; Heeger, A. J. *Nat. Mater.* **2012**, *11*, 44.
(9) van der Poll, T. S.; Love, J. A.; Nguyen, T. Q.; Bazan, G. C. *Adv. Mater.* **2012**, *24*, 3646.
(10) Zhou, J.; Wan, X.; Liu, Y.; Zuo, Y.; Li, Z.; He, G.; Long, G.; Ni, W.; Li, C.; Su, X.; Chen, Y. *J. Am. Chem. Soc.* **2012**, *134*, 16345.
(11) Shang, H.; Fan, H.; Liu, Y.; Hu, W.; Li, Y.; Zhan, X. *Adv. Mater.* **2011**, *23*, 1554.
(12) Liu, Y.; Wan, X.; Wang, F.; Zhou, J.; Long, G.; Tian, J.; Chen, Y. *Adv. Mater.* **2011**, *23*, 5387.
(13) Liu, Y.; Wan, X.; Wang, F.; Zhou, J.; Long, G.; Tian, J.; You, J.; Yang, Y.; Chen, Y. *Adv. Eng. Mater.* **2011**, *1*, 771.
(14) Lee, O. P.; Yiu, A. T.; Beaujuge, P. M.; Woo, C. H.; Holcombe, T. W.; Millstone, J. E.; Douglas, J. D.; Chen, M. S.; Frechet, J. M. *Adv. Mater.* **2011**, *23*, 5359.
(15) Liu, J.; Walker, B.; Tamayo, A.; Zhang, Y.; Nguyen, T.-Q. *Adv. Funct. Mater.* **2012**, *23*, 47.
(16) Loser, S.; Bruns, C. J.; Miyauchi, H.; Ortiz, R. P.; Facchetti, A.; Stupp, S. I.; Marks, T. J. *J. Am. Chem. Soc.* **2011**, *133*, 8142.
(17) Walker, B.; Tamayo, A. B.; Dang, X.-D.; Zalar, P.; Seo, J. H.; Garcia, A.; Tantiwiwat, M.; Nguyen, T.-Q. *Adv. Funct. Mater.* **2009**, *19*, 3063.
(18) Huang, J.; Jia, H.; Li, L.; Lu, Z.; Zhang, W.; He, W.; Jiang, B.; Tang, A.; Tan, Z.; Zhan, C.; Li, Y.; Yao, J. *Phys. Chem. Chem. Phys.* **2012**, *14*, 14238.
(19) Lee, J.; Han, A. R.; Hong, J.; Seo, J. H.; Oh, J. H.; Yang, C. *Adv. Funct. Mater.* **2012**, *22*, 4128.
(20) Lee, J.; Yun, M. H.; Kim, J.; Kim, J. Y.; Yang, C. *Macromol. Rapid Commun.* **2012**, *33*, 140.
(21) Ripaud, E.; Demeter, D.; Rousseau, T.; Boucard-Cétol, E.; Allain, M.; Po, R.; Leriche, P.; Roncali, J. *Dyes Pigm.* **2012**, *95*, 126.
(22) Tamayo, A. B.; Tantiwiwat, M.; Walker, B.; Nguyen, T. Q. *J. Phys. Chem. C* **2008**, *112*, 15543.
(23) Tamayo, A. B.; Walker, B.; Nguyen, T. Q. *J. Phys. Chem. C* **2008**, *112*, 11545.
(24) Tantiwiwat, M.; Tamayo, A.; Luu, N.; Dang, X. D.; Nguyen, T. Q. *J. Phys. Chem. C* **2008**, *112*, 17402.
(25) Ma, W. L.; Yang, C. Y.; Gong, X.; Lee, K.; Heeger, A. J. *Adv. Funct. Mater.* **2005**, *15*, 1617.
(26) Padinger, F.; Rittberger, R. S.; Sariciftci, N. S. *Adv. Funct. Mater.* **2003**, *13*, 85.
(27) Jo, J.; Kim, S.-S.; Na, S.-I.; Yu, B.-K.; Kim, D.-Y. *Adv. Funct. Mater.* **2009**, *19*, 866.
(28) Li, G.; Shrotriya, V.; Huang, J.; Yao, Y.; Moriarty, T.; Emery, K.; Yang, Y. *Nat. Mater.* **2005**, *4*, 864.
(29) Lee, J. K.; Ma, W. L.; Brabec, C. J.; Yuen, J.; Moon, J. S.; Kim, J. Y.; Lee, K.; Bazan, G. C.; Heeger, A. J. *J. Am. Chem. Soc.* **2008**, *130*, 3619.
(30) Salim, T.; Wong, L. H.; Bräuer, B.; Kukreja, R.; Foo, Y. L.; Bao, Z.; Lam, Y. M. *J. Mater. Chem.* **2011**, *21*, 242.
(31) Zhou, E. J.; Cong, J. Z.; Wei, Q. S.; Tajima, K.; Yang, C. H.; Hashimoto, K. *Angew. Chem., Int. Ed.* **2011**, *50*, 2799.
(32) Liu, X.; Sun, Y.; Perez, L. A.; Wen, W.; Toney, M. F.; Heeger, A. J.; Bazan, G. C. *J. Am. Chem. Soc.* **2012**, *134*, 20609.
(33) Janietz, S.; Bradley, D. D. C.; Grell, M.; Giebeler, C.; Inbasekaran, M.; Woo, E. P. *Appl. Phys. Lett.* **1998**, *73*, 2453.
(34) Li, Y. F.; Cao, Y.; Gao, J.; Wang, D. L.; Yu, G.; Heeger, A. J. *Synth. Met.* **1999**, *99*, 243.
(35) He, Y. J.; Chen, H. Y.; Hou, J. H.; Li, Y. F. *J. Am. Chem. Soc.* **2010**, *132*, 5532.
(36) Huang, J.; Zhao, Y.; Ding, X.; Jia, H.; Jiang, B.; Zhang, Z.; Zhan, C.; He, S.; Pei, Q.; Li, Y.; Liu, Y.; Yao, J. *Polym. Chem.* **2012**, *3*, 2170.
(37) Luhman, W. A.; Holmes, R. J. *Adv. Funct. Mater.* **2011**, *21*, 764.
(38) Peet, J.; Kim, J. Y.; Coates, N. E.; Ma, W. L.; Moses, D.; Heeger, A. J.; Bazan, G. C. *Nat. Mater.* **2007**, *6*, 497.
(39) Chu, T. Y.; Song, O. K. *Appl. Phys. Lett.* **2007**, *90*, 203512.
(40) Huang, J.; Zhao, Y.; He, W.; Jia, H.; Lu, Z.; Jiang, B.; Zhan, C.; Pei, Q.; Liu, Y.; Yao, J. *Polym. Chem.* **2012**, *3*, 2832.
(41) Malliaras, G. G.; Salem, J. R.; Brock, P. J.; Scott, C. *Phys. Rev.B* **1998**, *58*, 13411.
(42) Natali, D.; Sampietro, M. *J. Appl. Phys.* **2002**, *92*, 5310.
(43) Beaujuge, P. M.; Frechet, J. M. J. *J. Am. Chem. Soc.* **2011**, *133*, 20009.
(44) Facchetti, A. *Chem. Mater.* **2011**, *23*, 733.
(45) Yan, H.; Chen, Z. H.; Zheng, Y.; Newman, C.; Quinn, J. R.; Dotz, F.; Kastler, M.; Facchetti, A. *Nature* **2009**, *457*, 679.
(46) Yang, X. N.; Loos, J.; Veenstra, S. C.; Verhees, W. J. H.; Wienk, M. M.; Kroon, J. M.; Michels, M. A. J.; Janssen, R. A. J. *Nano Lett.* **2005**, *5*, 579.
(47) Gunes, S.; Neugebauer, H.; Sariciftci, N. S. *Chem. Rev.* **2007**, *107*, 1324.